Fault-controlled contaminant plume migration: Inferences from SH-wave reflection and electrical resistivity experiments

Article *in* Journal of Applied Geophysics · July 2018

DOI: 10.1016/j.jappgeo.2018.07.007

CITATIONS
2

READS
105

2 authors:

Ali Almayahi
University of Basrah
11 PUBLICATIONS **13** CITATIONS
SEE PROFILE

Edward Woolery
University of Kentucky
114 PUBLICATIONS **669** CITATIONS
SEE PROFILE

Journal of Applied Geophysics 158 (2018) 57–64

Contents lists available at ScienceDirect

Journal of Applied Geophysics

journal homepage: www.elsevier.com/locate/jappgeo

Fault-controlled contaminant plume migration: Inferences from SH-wave reflection and electrical resistivity experiments

Ali Almayahi [a,b,*], Edward W. Woolery [a]

[a] Department of Earth and Environmental Sciences, University of Kentucky, Lexington, KY 40506-0053, USA
[b] Department of Geology, University of Basra, Basra, Iraq

ARTICLE INFO

Article history:
Received 20 April 2018
Received in revised form 20 July 2018
Accepted 21 July 2018
Available online 25 July 2018

ABSTRACT

A contaminant plume migrates within a shallow late-Tertiary gravel aquifer in an anomalous curvilinear pattern aligned with the general orientation of an underlying early-Paleozoic fault system. The bedrock faults are masked by ~100-m of overlying Late Cretaceous through Quaternary sediment. Fault reactivation has been as late as Pleistocene with near-surface deformation affecting the aquifer. Near-surface geophysical attributes indicate a potential structural influence for the anomalous plume migration pattern. Specifically, the fault zones exhibit lower shear-wave velocity (100 m/s) and electrical resistivity (80 Ω-m) relative to surrounding sediment. In addition, shear-wave splitting across a well-constrained fault strand indicates the sediment has an average 3.6% azimuthal anisotropy coincident with fault strike. Variation in elastic and electrical properties, as well as spatial coincidence of the plume and geologic structure, suggest neither mechanical (i.e., consolidation) nor chemical (i.e., cementation) "healing" of the sediments have completely occurred since deformation cessation. The variation in geophysical characteristics are also indicative of a non-uniform hydraulic conductivity, thus providing a structurally controlled preferential pathway for fluid migration. These results demonstrate that integrated non-invasive geophysical methods are effective for evaluating complex geologic conditions in environmentally sensitive areas.

1. Introduction

Construction of facilities at Paducah Gaseous Diffusion Plant (PGDP) in western Kentucky (Fig. 1) and other sites in the United States for enriching uranium via gaseous diffusion of uranium hexafluoride began in the 1950s. Prior to its enrichment mission, the PGDP site served as a trinitrotoluene ordnance factory during World War II (Clausen et al., 1992). The prevailing standards-of-practice during this long history of industrial chemical activity at the site caused unfavorable environmental conditions. The 14-km^2 site is now undergoing decontamination and decommissioning after operating for more than 70 years. The critical environmental concerns began in the late 1980s when elevated concentrations of facility-derived trichloroethylene (TCE), a common cleaning solvent, and technetium-99 (Tc-99), a fission by-product introduced through the reprocessing of nuclear reactor tailings, appeared in privately owned groundwater wells located approximately 1.5 km north of the plant site (Clausen et al., 1992). This discovery generated a series of environmental investigations designed to determine the source and extent of groundwater contamination. A considerable part of the work was devoted to improving the geologic framework model. Collectively, more than 900 boreholes and observation wells were drilled into the ~100 m of unlithified sediment overlying carbonate bedrock (Sexton, 2006). The drilling was widely distributed across the site; however, most of the boreholes were limited to depths not exceeding a few tens of meters (i.e., Tertiary aquifer). This was in order to minimize the potential for deeper vertical cross contamination (Sexton, 2006; Woolery et al., 2009). Although the lack of full overburden sampling in the borehole dataset precluded a more complete post-Paleozoic geologic model, the invasive measurements did show the aquifer's contaminant plume as having an unusual migration pattern (Fig. 2). Specifically, the plume consists of two northeast-oriented, relatively narrow, curvilinear arms migrating from the facility toward the west-flowing Ohio River. Initial interpretations for the complex flow pattern were associated with the aquifer's depositional and erosional environment. This was in part contrary to the expected hydrogeologic gradient, wherein preserved paleochannels in the aquifer were acting as preferential pathways for groundwater flow and contaminant transport. Follow up groundwater models, however, suggested paleochannels were likely not influencing flow and migration pathways, because the hydraulic conductivity contrast between the

* Corresponding author at: Department of Earth and Environmental Sciences, University of Kentucky, Lexington, KY 40506-0053, USA.
E-mail addresses: azal222@g.uky.edu (A. Almayahi), woolery@uky.edu (E.W. Woolery).

https://doi.org/10.1016/j.jappgeo.2018.07.007
0926-9851/

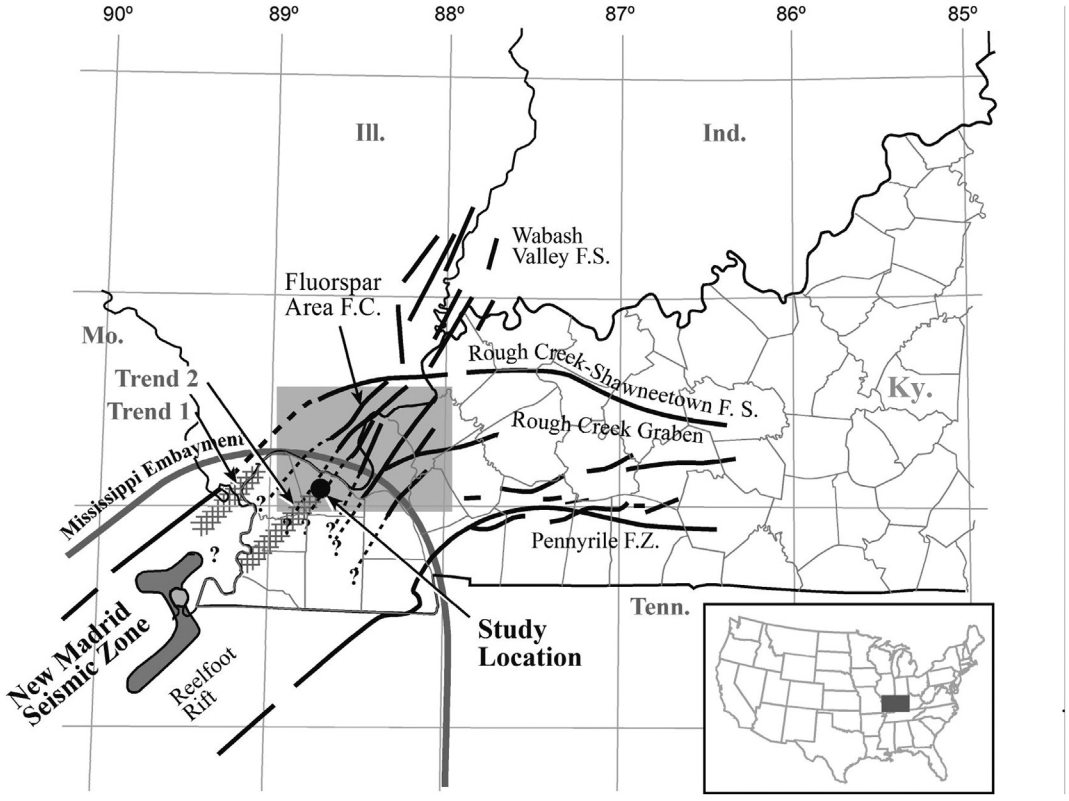

Fig. 1. Seismotectonic structures in the central United States (inset). The Mississippi embayment sediment fill masks the bedrock structures. The New Madrid seismic zone is in the dark shaded area within the Reelfoot rift. The trend 1 and 2 cross-hatched pattern represents diffuse seismicity extending from the central seismic zone to near the northern embayment boundary. The study location is at the junction between Reelfoot rift and Rough Creek graben, near the terminus of the diffuse trend (2) of seismicity. The shaded rectangle around the study location is the area of Fig. 2.

channel and non-channel sediment is not significant in this particular hydrogeologic setting (Clausen et al., 1992).

In order to improve (non-invasively) the geologic model, a series of shear-wave reflection profiles, totaling ~17.5 km, provided high-quality images of the post-Paleozoic stratigraphy and transitions. These data also revealed an underlying early-Paleozoic fault complex that has been Quaternary-active, thus affecting the hydraulic conductivity of the gravel aquifer. As part of their seismic hazards evaluation, Woolery et al. (2009) explicitly constrained the cessation of the local neotectonic deformation between 16 and 25 kya. For this study, we reconsider the coincident single and multicomponent S-wave seismic reflection data, as well as electrical resistivity tomography data in an environmental context. Specifically, we address the questions: can near-surface structural features within unlithified sediment locally influence hydraulic conductivity and act as a preferential pathway for fluid migration, or given fault dormancy of a few tens of thousands of years, has geomechanical (consolidation) and/or have geochemical (cementation) processes "healed" the neotectonic deformation zones in a manner suppressing or negating migration bias.

2. Geologic setting

The PGDP is located adjacent to the Ohio River and within the northern part of the Mississippi embayment, an elongate southwest-plunging sediment-filled basin (Fig. 1). The embayment overlies the intersecting late Precambrian–early Paleozoic Reelfoot rift and Rough Creek graben. A northeast-oriented structural accommodation zone, called the Fluorspar Area fault complex (FAFC), is located at the northern juncture of the two rift systems. Immediately outside of the embayment's nearby northern boundary, the bedrock-exposed FAFC is described as a series of strike-slip pull-apart grabens bounded by N20°E- to N40°E-striking normal and inverted reverse faults extending into the Quaternary (Fig. 2) (Nelson et al., 1999). These fault strands project beneath the PGDP where the embayment sediments mask their bedrock expression (Woolery and Street, 2002). Woolery et al. (2009) corroborated the continuation of the FAFC beneath the PGDP, and temporally defined the reactivated fault displacement as late Pleistocene.

The top of the Mississippian limestone bedrock is an unconformity, stratigraphically overlain by ~100 m of unlithified sediments that are Late Cretaceous and younger (Clausen et al., 1992; Woolery and Street, 2002; Sexton, 2006) (Fig. 3). Regionally, undifferentiated interbedded-banded Late Cretaceous and Paleocene sands and clays belonging to the McNairy and Clayton Formations rest directly on the Mississippian bedrock (Nelson et al., 1999). Undifferentiated Eocene silty sands and clays unconformably overlie the Clayton-McNairy. Pliocene–Pleistocene sands and gravels locally referred to as the Continental Deposits (or alternatively, Mounds Gravel and Metropolis Formation) separate the Eocene sands–clays and surficial Pleistocene loess. The Continental Deposits are the framework sediment for the local aquifer. The loess consists primarily of silts deposited during periodic glaciation through the Pleistocene (Nelson et al., 1999). The tops of the bedrock, Cretaceous, and lower Continental Deposits are high acoustic impedance boundaries, and define the primary seismic-reflection marker horizons (Woolery and Street, 2002).

3. Geophysical methods

3.1. General SH-wave seismic reflection acquisition and processing

Seismic refraction and reflection methods for hydrogeophysical assessments generally use P-wave energy for distinguishing between unsaturated and saturated horizons in groundwater mapping studies (Garambois et al., 2002). Compressional-wave velocity is also used to estimate field porosity conditions based on poroelasticity theory and

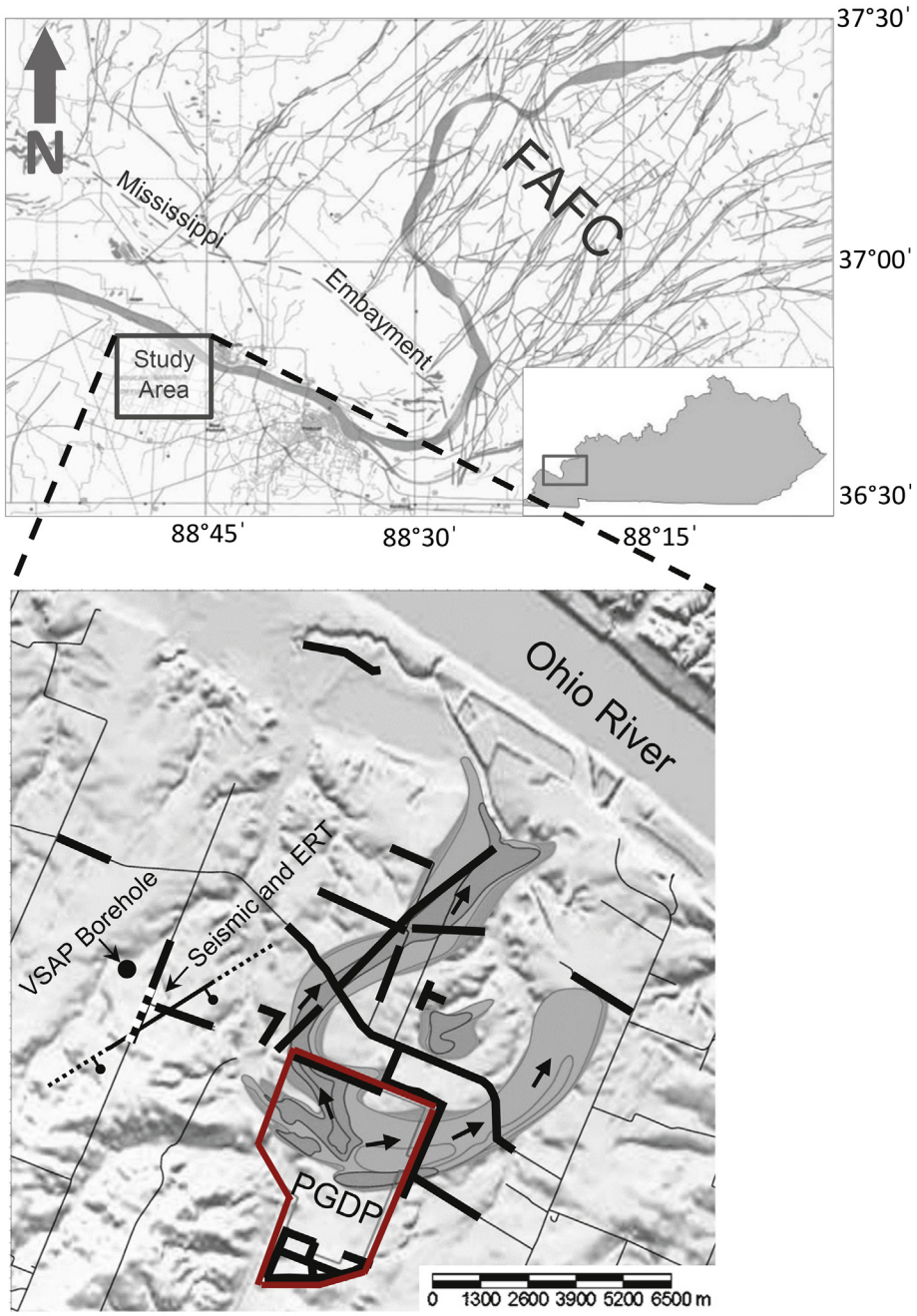

Fig. 2. The study location is adjacent to the locally northwest flowing Ohio River in the northernmost Mississippi embayment. The outcrop mapped Fluorspar Area fault complex location and orientation is north of the embayment boundary (top). The expanded view of the study area (bottom) shows the seismic-reflection data set (heavy black lines) relative to the anomalously migrating curvilinear contaminant plume (gray shaded area) and PGDP boundary (red outline). The bold black arrows define the plume flow direction. The topographic relief does not exhibit any geomorphic or surface expressions of reactivated transpressional faulting. The seismic and electrical resistivity experimental data (white-black dashed line) we discuss were collected over part of a longer reflection dataset. These data are adjacent with borehole VSAP and located southwest of the main plume across a well-constrained fault, shown by the thin black line with dashed ends. The "stick and ball" symbols are located on the fault downthrow or footwall. (For interpretation of the references to colour in this figure legend, the reader is referred to the web version of this article.)

the Biot-Gassman equations (Adelinet et al., 2017). However, using P-wave energy for near-surface seismic imaging in saturated sediments often yields poor results due to the groundwater "masking" effect of the reflection signal in these relatively low-velocity high-void-ratio solids (e.g., Woolery et al., 1993; Deidda and Balia, 2001; Woolery and Street, 2002; Woolery et al., 2009; Stucchi et al., 2017; among others). The unlithified near-surface fluvial and alluvial environments at the PGDP site are typical of these conditions. Conversely, shear-wave (SH mode) energy can be a more responsive approach for obtaining geological images in water-saturated sediments, because as "framework waves" they are constrained to propagate in solid media. Although S-waves can have frequency content only one-half to one-third that of P-waves, the P-wave velocities, particularly in the embayment sediment, can be five to 10 times higher than S-waves; therefore, resolution improves by a factor of 2 to 3 using S-waves (Harris, 1996; Woolery and Almayahi, 2014). Our data have ~50 Hz dominant signal and a velocity range between 150 and 500 m/s. This yields a resolvable vertical limit ranging between 0.75 m and 2.2 m. The detectable limits are considerably smaller (i.e., 1/8 λ to 1/20 λ, where λ is the dominant wavelength). The spatial or horizontal resolution, based on the radius of the first Fresnel zone, is constrained between approximately two and four shot points.

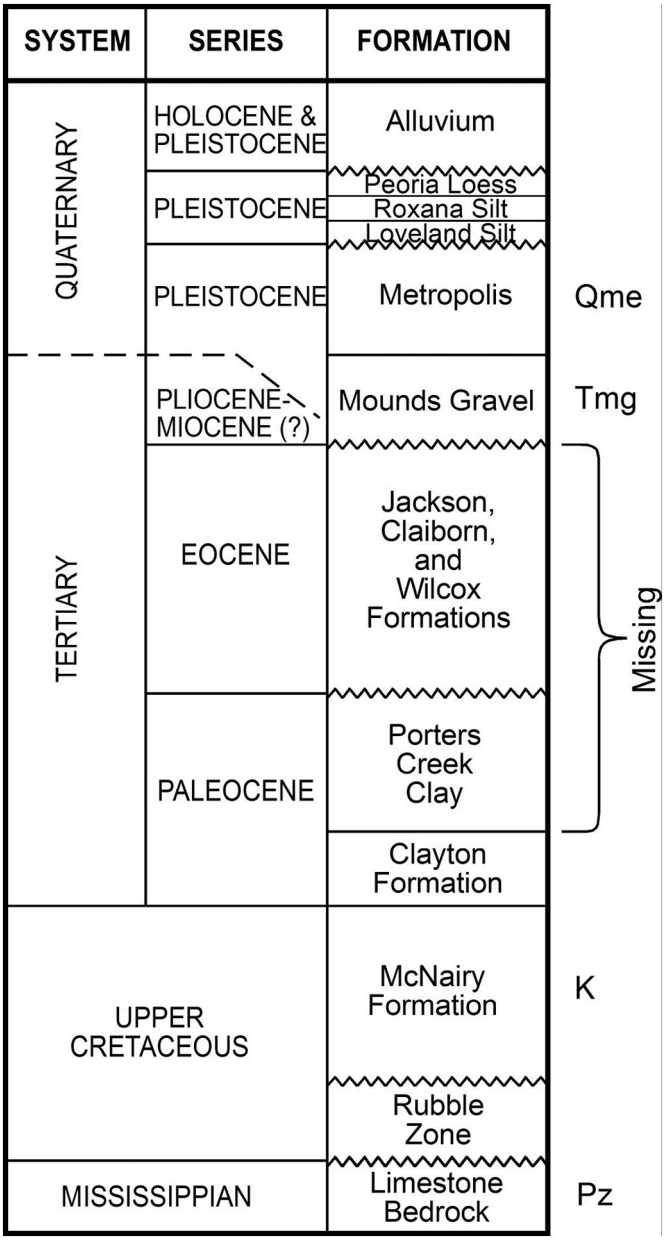

Fig. 3. Approximately 100 m of unlithified Cretaceous through Quaternary sediments unconformably overlie Mississippian limestone bedrock (modified from Woolery and Almayahi, 2014). The tops of the Pz, K, Tmg, and Qme are the primary impedance boundaries and are at borehole depths of 18, 25, 50, and 105 m, respectively. The stratigraphic depths are used to constrain the seismic reflection correlation. Given the uncertainty in the velocity model and near equivalent surface elevations, the resultant correlations are excellent.

A 48-channel 24-bit engineering seismograph recorded all seismic data. The energy source for SH-wave data was three to five horizontal impacts of a 1.4 kg hammer on a 3-kg modified H-pile section oriented perpendicular to the spread with its flanges set in similarly sized trench excavations to maximize the energy couple. The hold-down weight of the H-pile was between approximately 70 and 80 kg, including the hammer swinger and source. Double-sided impacts and correlative seismograph polarity reversals enhanced S-wave energy. All SH-wave reflection surveys used single-component horizontally polarized 30-Hz geophones. The common midpoint (CMP) acquisition parameters used a 2-meter geophone and shot station spacing. Data processing was with a PC-based commercial software, following a standard procedure that included coherent noise muting, digital filtering, trace editing, appropriate trace balancing, iterative velocity analyses, surface consistent statics, and post-stack Kirchhoff migration. Table 1 provides detailed parameters for the seismic-reflection acquisition and processing. Fig. 4 provides an example series of pre-stack processing stages for: (1) raw, (2) filtered/balanced/muted, and (3) moved out gathers.

3.2. SH-wave birefringence measurement

Woolery and Almayahi's (2014) S-wave splitting data are composed of 24 orthogonal pairs of horizontal single-component geophones, as well as similarly aligned orthogonal energy source orientations per shot station. Data acquisition was initiated in a transverse-source–transverse-receiver (TT) and transverse-source–radial-receiver (TR) orientation at each receiver and shot station; however, prior to "rolling" to the next station, the source was rotated 90°, simultaneously recording the radial-source–transverse-geophone (RT) and radial-source–radial-geophone (RR) data. The data were processed with the standard CMP procedures as described above, but prior to the velocity analysis, matrices of gathers were rotated to determine the "fast" (S1) and "slow" (S2) shear-wave directions (i.e., natural coordinate system) following the procedures described by Harris (1996). Rotation of each component (i.e., TT, TR, RT, and RR) was in 5° increments, between 0° and 180° clockwise, and amplitude spectra, along with their ratio difference calculated for each rotation dataset. The resultant natural coordinate system aligns the maximum (S1) and minimum (S2) energy parallel and orthogonal to the inclusion bearing, respectively. The natural coordinate rotated gather files were subsequently CMP processed the same. The resultant time delay or dynamic mis-tie between the S1 and S2 directions were a measure of azimuthal anisotropy (Martin and Davis, 1987):

$$\eta = \frac{T_{fast} - T_{slow}}{T_{fast}} \times 100\% \quad (1)$$

Where, η is azimuthal anisotropy and T_{fast} and T_{slow} are the reflected signal's two-way-travel-times in the S1 and S2 natural coordinates, respectively.

Additional detail for the acquisition and processing procedures are in Woolery and Almayahi (2014).

3.3. Electrical-resistivity acquisition and processing

Electrical-resistivity tomography (ERT) surveys were acquired coincident with segments of four SH-wave seismic reflection profiles. We discuss one of the four lines as part of our objectives for this study. The initial purpose for all the ERT lines was to test the ability of electrical methods to resolve the faulted sediments in the local environment. The

Table 1
Signal processing procedures for the seismic reflection data.

	Processing Functions	Parameters
1	Reformat	Convert the data from SEG-2 to VISTA12 internal format
2	Geometry	Geometry definition
3	Time-Variant Scaling	Scale: 1.000 RMS Trim Median
4	Data Scaling	Scale: 1.000 Mean Scale
5	Ormsby Band-Pass	20.00/30.00–75.00/85.00 Hz
6	FK_Filter	F-K Designed Filter File Power: 1.00
7	Adaptive Subtraction	Time Domain Adaptive Subtraction
8	Ormsby Band-Pass	20.00/30.00–75.00/85.00 Hz
9	Normal Move-Out	Velocity Percent: 100.00%
10	Muting	Taper Mute Zones by 4 Samples
11	Statics Shifts	Combined Static: STATIC_TOTAL
12	Noise Attenuation	2D/3D Threshold Median Noise Attenuation/Replacement
13	Common Mid-Points Stack	Stack: No Normalization of Stack CMP Stack
14	Post stack Depth Migration	Smoothers Time: 1.000 ms BinTop: 50 Bin Bottom: 300

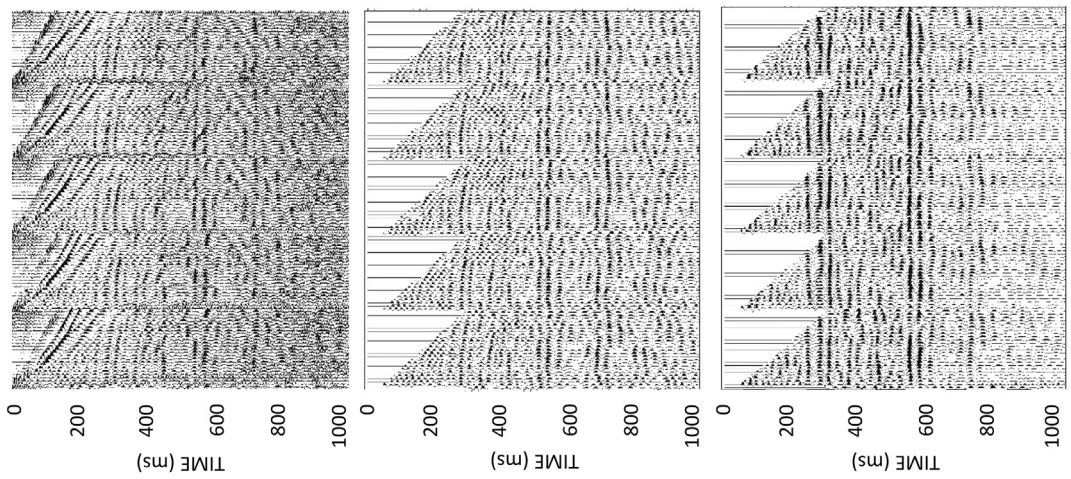

Fig. 4. Example series of SH-wave reflection gathers located near CMP station 325 (see Fig. 5): gained (top), muted (middle) and moved out (bottom).

ERT system included a single-channel switching capability for 56 stainless-steel electrodes, and 4 passive cables. The electrodes directly coupled to the ground and attached to the passive cables with a spring collar. The dipole-dipole array, generally considered optimally sensitive to lateral variations, was the acquisition configuration for imaging the near-vertical faults. The array used a 6-m electrode spacing and moved, or "rolled-along," in order to extend the survey line lengths. The acceptable error percentage between any two measurements was 2%. The electrical resistivity data were processed and inverted into 2D electrical resistivity tomography (ERT) profiles using commercial software. The main goal is an accurate fit of the resultant inversion model with the measured field data. Three inversions algorithms were available: damped least squares, smooth model inversion, and robust least-squares inversion. The robust least-squares inversion minimized the absolute value of data misfit, and was efficient for removing noise from the desired signal (Dahlin and Zhou, 2004). In geologic conditions with sharp boundaries and fault-like features as survey targets, the robust least-squares inversion generally provides better results. Smoothing and damping factors were set to avoid over-smoothing the resultant model. A horizontal and vertical roughness ratio of 1.5 enhanced the effect of lateral variations along the profile. Table 2 provides the specific acquisition and processing details.

Table 2
Inversion parameters for the 2D electrical resistivity data.

Initial settings		
Minimum voltage (mV)	0.2	
Minimum absolute (V/I)-ohm	0.0005	
Maximum repeat error	3%	
Minimum apparent resistivity (ohm-m)	1	
Maximum apparent resistivity (ohm-m)	10,000	
Maximum reciprocal error	5	
Inversion method	Robust inversion	
Forward modeling settings		
Forward modeling method	Finite element	
Forward equation solver	Cholesky decomposition	
Type of boundary condition	Dirichlet	
Number of mesh divisions	2	
Thickness incremental factor	1.1	
Depth factor	1.1	
Resistivity inversion settings		
Number of iterations	Stop criteria	8
Maximum RMS error		2%
Error reduction		5%
Smoothing factor/damping factor	10	
Starting model	Average apparent resistivity	
Model parameter width	1	
Model parameter height	1	
Resolution	0.2	
Horizontal/vertical roughness ratio	0.5–2.0	

4. Discussion

The available PGDP dataset includes ~17.5 km of seismic reflection lines, as well as four ERT lines and one multi-component S-wave birefringence survey. Initially, the ERT and seismic reflection data evaluated the response and resolution variability of these techniques for this particular environment; however, for evaluating the potential structural control of fluid migration, we discuss one seismic reflection line, one ERT line, and the single shear-wave splitting survey. Woolery and Almayahi (2014) collected the S-wave splitting survey to determine if birefringence existed, and if so, could the associated near-surface azimuthal anisotropy accurately determine structural orientation in unlithified sediment lacking surface expression. They used a well-constrained fault target because many geologic processes or factors (e.g., depositional fabric, mineralogy, differential stress, heat flow, fractures, faults, etc.) can induce anisotropy (Crampin, 1985). These data were located up gradient of the contaminant plume and near a borehole log (VSAP) with the complete post-Paleozoic stratigraphy available for geophysical correlation. Moreover, these data effectively constrained and characterized the structural style and near-surface extent of the neotectonics (Fig. 2). The SH-wave CMP reflection and S-wave splitting seismic lines, along with the one ERT profile represent a complete suite of data for our experimental objectives (Fig. 2). These data have high-quality signal and provide the necessary fault characteristic constraints, including a known strike and an observable displacement image across the entire resolvable stratigraphic section. The seismic data consist of coincident SH-wave CMP single-component and multi-component S-wave splitting profiles. The S-wave splitting profile is shorter, focusing on the fault-affected area. The ERT survey is also coincident with the larger SH-wave CMP line.

Time and converted depth images for the part of the CMP profile across the well-constrained fault are in Fig. 5. Borehole VSAP (Fig. 3) provides constraint for the seismostratigraphic correlation. The interpreted fault zone is between CMP stations 150 and 250. Woolery and Street (2002) interpreted this particular fault strand as displacing the tops of Paleozoic (Pz) bedrock, Cretaceous (K) Clayton-McNairy, and Mounds Gravel (Tmg). Our reprocessed depth-converted profile supports the original interpretation and suggests displacements across the Pz, K, and Q are approximately 25 m, 14 m, and 4 m, respectively. The overall sense of deformation is normal dip slip in the Pz and K section; however, the shallowest reflected horizons exhibit a reversed sense of displacement, indicating later transpressional behavior.

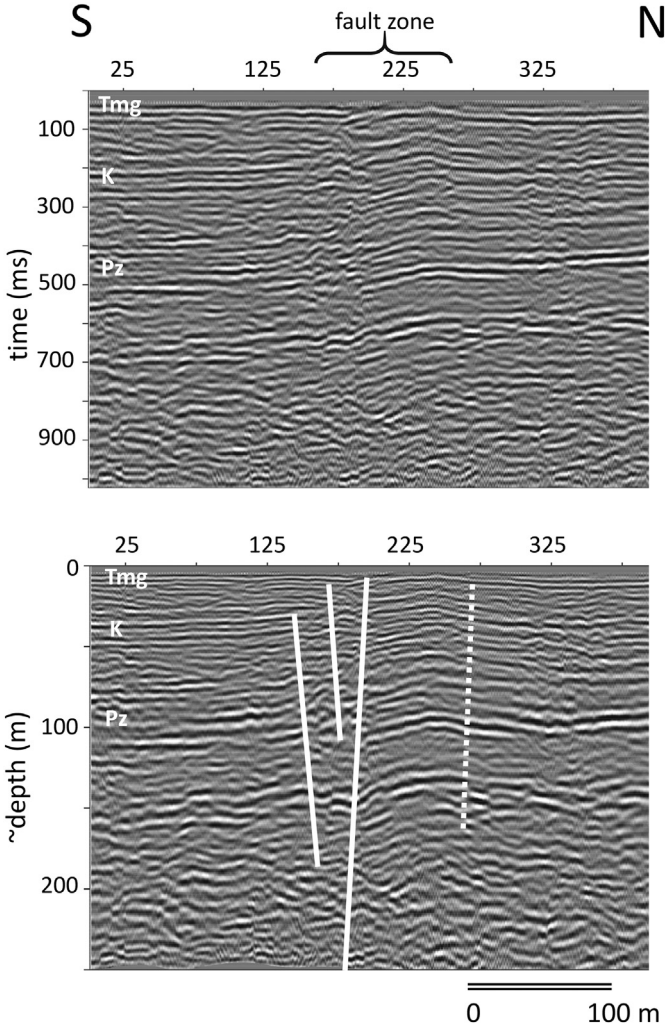

Fig. 5. Final SH-wave CMP image of the well constrained northeast oriented fault zone. The time (top) and depth converted (bottom) images have the major reflection boundaries labeled. The stratigraphic horizons in the depth converted profile correlate well with the nearby VSAP borehole. The Pz, K, and Tmg horizons exhibit approximately 25, 14, and 4 m of offset, respectively. Displacement in the shallowest horizons appear inverted, indicative that the initial high-angle normal faults have been reactivated in the later east-west oriented compressional stress field as transpressional structure (Woolery and Street, 2002; Woolery et al., 2009).

Woolery et al. (2009) further defined the temporal characteristics of the faults at the PGDP. In a set of nearby along-strike faults, they found deformation extending to within 7 m below the ground surface. Eighty-six closely spaced and continuous core samples, along with 12 optical stimulated luminescence measurements across the deformation zone indicated the latest fault displacement occurred between 16.6 and 23.5 ka.

The lack of Holocene movement led to the speculative idea of geomechanical or geochemical restoration or "healing" of the deformation zones in a manner that would suppress or negate any fault influence on hydraulic conductivity, thus preferential fluid migration pathways. We use integrated high-quality seismic and electrical data at a well-constrained fault location to test this hypothesis.

Woolery and Almayahi (2014) performed additional seismic reflection profiling adjacent to the seismic lines herein, thus establishing the well-constrained fault parameters. Subsequently, they acquired 4-component shear-wave reflection data coincident with the fault identified in our CMP line as an initial search for the presence of birefringence and a means of determining near-surface orientation for structures without surface expression. They calculated the difference in the normalized spectral ratios for cross-diagonal and main-diagonal elements of each rotation within the shear-wave window (see Woolery and Almayahi, 2014 for specific details). This resulted in a 40° fast direction (maximum energy) and 130° slow direction (minimum energy) relative to line direction (Fig. 6). These orthogonal directions defined the natural coordinates and translated to N 60° E and N 30° W bearings, respectively. The N 60° E maximum energy compared to their measured N 61° E fault strike. In addition, between 9.5 and 15 ms of dynamic mistie was determined between the near-surface and bedrock two-way-travel-time signal, respectively (Fig. 6). This correlated to an average 3.6% azimuthal anisotropy, suggesting a significant deformation influence (i.e., microfractures) remains. The elastic anisotropy associated with geologic structure also suggests potential influence or effects in other physical attributes, such as hydraulic conductivity, and manifesting as a preferential fluid migration pathway.

The inverted dipole-dipole ERT profile across the target fault yielded a 50-m maximum sampling depth, approximately half of the post-Paleozoic sediment stratigraphy (Fig. 7). The total length of the ERT line is 500 m, with approximately 400 m having complete depth sampling. The upper 6 m show relatively low resistivity values, varying slightly between ~15 and 25 Ω-m. This is consistent with elevated water content in the fine-grained loess deposits. The increased resistivity below 6 m correlates reasonably well with the top of the Metropolis Formation (Qme) as found in borehole VSAP (Fig. 3). The resistivity in this silty sand and gravel deposit varies between ~30 and 80 Ω-m. Less resistive conditions associated with the Mounds Gravel (Tmg) appear below this higher resistivity zone. The erosional boundary yields a highly irregular geophysical contact at approximately 15-m depth below ground surface. The depth and irregular surface is consistent with the depth-converted seismic reflection image. The ERT sampling depths also overlap the logged borehole depth for the top of the Cretaceous Clayton-McNairy Formation; however, a distinct boundary is not observed. This is not an unanticipated electrical response for the thick saturated sands and banded clays comprising the Clayton-McNairy. The ERT image exhibits a coherent signal for the Continental Deposits along the southern part of the profile, between stations 0 and 200. Truncation of the coherent resistive signal by a distinct zone of less coherent, higher conductivity material is observed between stations 200 and 300. This zone is approximately 100-m wide. Moreover, a vertical down-to-the-south offset occurs across this electrical discontinuity. This anomalous electrical zone spatially correlates to the ~100-m wide fault zone interpreted in the seismic reflection profile, between CMP stations 150 and 250. In addition, ERT station 240 has the lowest observed resistivity measurements along the profile, and spatially correlates with the primary fault strand interpreted on the seismic image. The S-wave velocity model overlaying the stacked CMP image in Fig. 7 also indicates the approximately 100-m-wide fault zone has a significantly lower (~100 m/s) S-wave velocity than the surrounding area.

The contrasting electrical and elastic parameters in the interpreted fault zone compared with the surrounding area suggest neither a geomechanical nor geochemical restoration (or "healing") to uniform physical conditions has occurred. Moreover, the lower S-wave velocity and azimuthal anisotropy measurements within the fault zone indicate a preferentially oriented zone of weakness, and the significantly lower electrical resistivity signify elevated fluid content. Consequently, we infer the sediments within the neotectonic structure have an overall higher hydraulic conductivity and can act as a preferential pathway for local fluid migration.

5. Conclusions

Prior neotectonic deformation has affected the local aquifer at the PGDP site, but has been dormant since between approximately 16 and 25 ka (Woolery and Street, 2002; Woolery et al., 2009). The extended period of structural latency generated speculative questions regarding the present effect the faults have on the aquifer's relative hydraulic conductivity within the fault zone. In particular, is the elevated hydraulic conductivity created in faulted sediment reduced (or eliminated) due

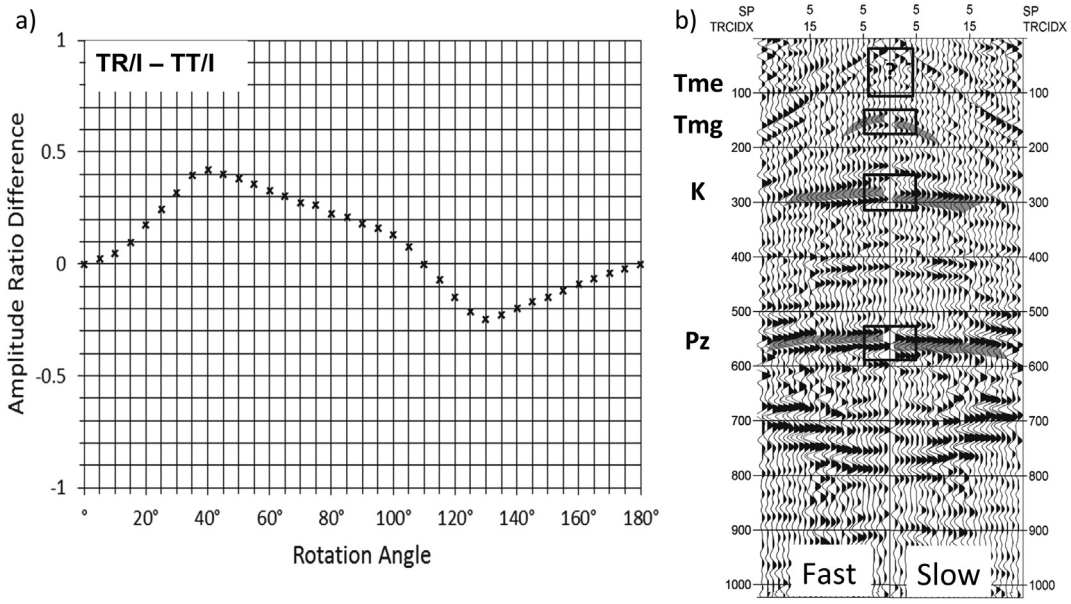

Fig. 6. a) The S-wave splitting experiment rotated the difference in the four-component spectral ratios every 5° to determine the fast and slow directions composing the natural coordinate system. b) Symmetric mirror view of a field-file seismogram from the same shot point that has been rotated into the fast and slow directions. The comparative two-way-travel-times show the dynamic mis-tie at the primary reflecting horizons (modified from Woolery and Almayahi, 2014).

to inertial mechanical consolidation and/or geochemical cementation given the long time interval since the last displacement, or is it preserved? Integrated geophysical measurements of a well-constrained fault exhibiting deformation across the resolvable subsurface sediment stratigraphy show significant variation in the elastic and electrical properties between deformed and undeformed sediments. Specifically, the shear-wave velocity and electrical resistivity within the fault zone exhibit a marked decrease of approximately 100 m/s and 80 Ω-m, respectively, compared with adjacent undeformed sediments. In addition, S-wave birefringence measurements detected azimuthal anisotropy in the unlithified sediment coincident to and aligned with the fault orientation. An average 11.3 ms dynamic mis-tie suggests a 3.6% azimuthal anisotropy between the top of bedrock and surface. This falls within the reasonable value range of 0.5 and 5% suggested by

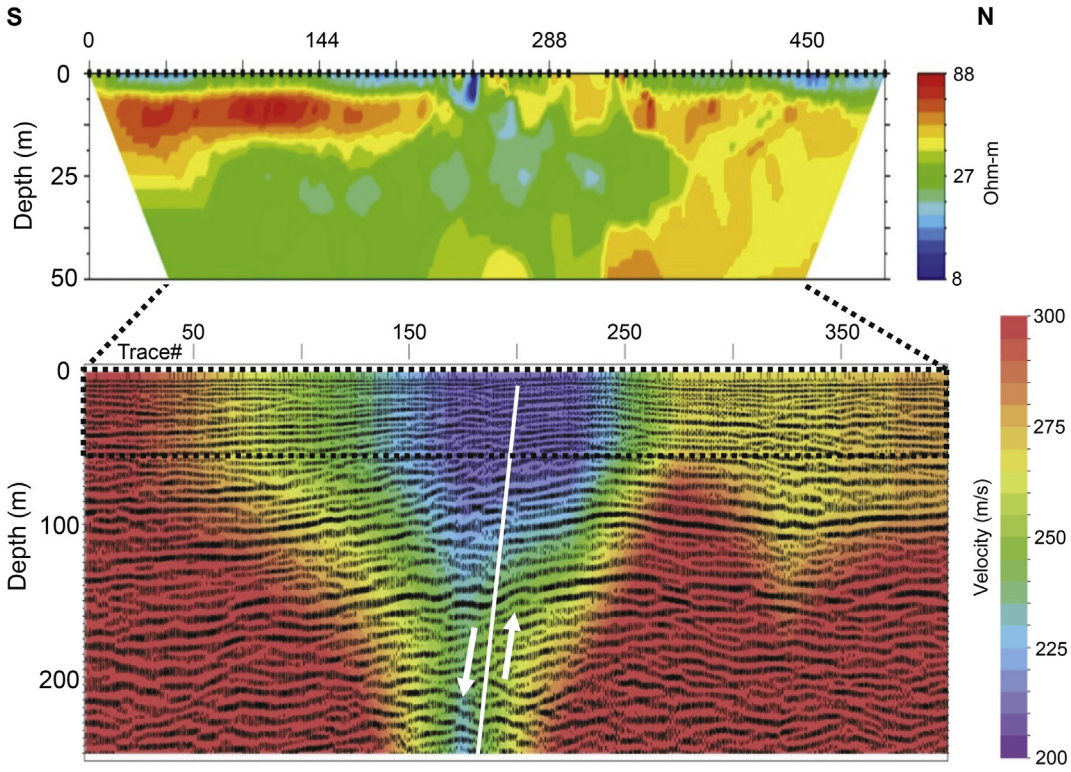

Fig. 7. A comparison of part of the SH-wave seismic-reflection and coincidentally acquired electrical resistivity images across the well-constrained fault zone. The ERT profile samples approximately half the site stratigraphy as defined by the black dashed outline. We show the associated seismic-velocity model overlaying the seismic profile. The S-wave velocity in the fault zone is approximately 100 m/s slower than the surrounding area. The ERT image exhibits as much as an 80 Ω-m reduction in resistivity within the fault zone relative to the surrounding undeformed sediments.

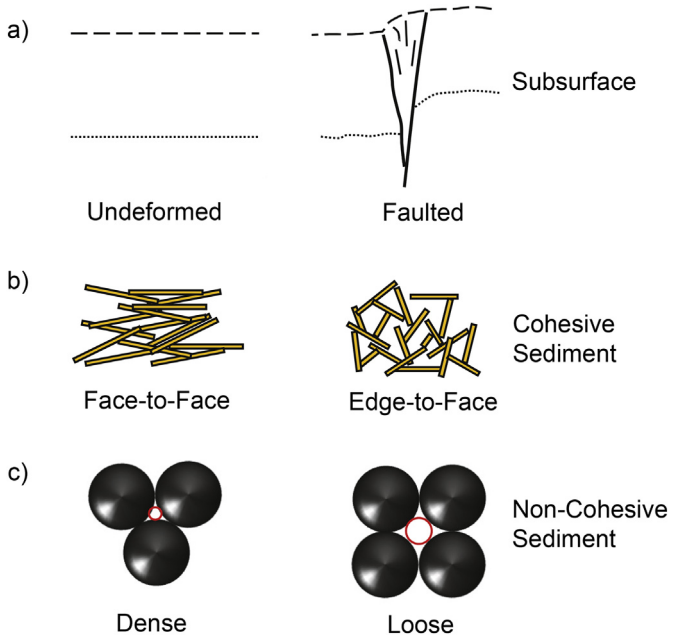

Fig. 8. Schematic representation of fault effects on the physical configuration of sediment particles. a) Quasi-brittle behavior of faulted unlithified stratigraphy. Predominantly non-cohesive sediments have elevated hydraulic conductivity along a fault surface, while primarily cohesive sediments can have a decrease in hydraulic conductivity due to clay "smearing" (Bense et al., 2003, 2013). However, secondary porosity due to micro-cracks in the sediment can enhance both. b) More importantly, cohesive (i.e. clay) sediments are deposited in low-energy environments where particles arrange in a denser "face-to-face" configuration; however, they can reorient to a higher void ratio, "edge-to-face," configuration in the broader fault damage zone. c) In addition, non-cohesive sediments undergoing enhanced hydraulic conductivity along the fault surface, can reorient from denser to looser packing configuration in the broader deformation zone depending on the initial conditions.

Crampin and Lovell (1991). We infer from the comparative variation in the collective geophysical properties for deformed and undeformed sediments (cohesive and non-cohesive) that geochemical or geomechanical alterations have not significantly diminished the hydraulic conductivity during the structural dormancy. This would maintain an increased sediment void ratio for preferential fluid and contaminant migration in the Tertiary gravel aquifer. Moreover, a fault-controlled preferential pathway provides a reasonable explanation and context for the curvilinear plume configuration anomalously migrating to the northeast, rather contrary to a more direct north orientation to the Ohio River that may be expected for a hydraulic gradient in a homogeneous isotropic granular aquifer. This interpretation also corroborates prior laboratory and field measurements within the deformation zone of faulted shallow crust, including near-surface sediments (Sanford, 1959). The sand-rich stratigraphy, in particular, indicates elevated hydraulic conductivity (Bense et al., 2003, 2013). Although the clay components can have reduced hydraulic conductivity along the fault surface due to "smearing," cohesive sediments in the broader damage zone can undergo a particle realignment to a more flocculated (or edge-to-face) configuration (Fig. 8).

The results do not eliminate the potential for mechanical (consolidation) and/or geochemical (cementation) processes "healing" the neotectonic deformation zones and suppressing or negating migration bias in other unlithified sediment environments, nor do they preclude partial healing at the PGDP site. The results do suggest any geomechanical or geochemical alterations present at the PGDP site are not mature. In addition, the results indicate an integrated non-invasive geophysical approach can be effective for evaluating complex geologic conditions in environmentally sensitive areas.

Acknowledgments

Financial support for this work was through the Department of Energy/Kentucky Research Consortium for Energy and Environment (Award DE-FG05-03OR23032) and the U.S. Geological Survey (Award 01HQGR0044). Additional support came from the Kentucky Geological Survey (KGS). The authors wish to thank two anonymous reviewers, as well as Co-Editor in Chief Jianghai Xia for their helpful comments and suggestions that significantly improved the manuscript.

References

Adelinet, M., Dominguez, C., Fortin, J., Violette, S., 2017. Seismic-refraction field experiments on Galapagos Islands: a quantitative tool for hydrogeology. J. Appl. Geophys. 148, 139–151.
Bense, V.F., Van den Berg, E.H., Van Balen, R.T., 2003. Deformation mechanisms and hydraulic properties in unconsolidated sediments; the Roer Valley rift system, the Netherlands. Hydrogeol. J. 11, 319–332.
Bense, V.F., Gleeson, T., Loveless, S.E., Bour, O., Schiebek, J., 2013. Fault zone hydrogeology. Earth Sci. Rev. 127, 171–192.
Clausen, J.L., Douthitt, J.W., Davis, K.R., Phillips, N.E., 1992. Groundwater Investigation Phase III for Paducah Gaseous Diffusion Plant, Paducah, Kentucky: A Final Report Prepared for the U.S. Department of Energy Under Contract No. DEAC0f76OR00001. Martin Marietta Energy Inc.
Crampin, S., 1985. Evaluation of anisotropy by shear-wave splitting. Geophysics 50, 142–152.
Crampin, S., Lovell, J., 1991. A decade of shear-wave splitting in the Earth's crust: what does it mean? What use can we make of it? And what should we do next? Geophys. J. Int. 107, 387–407.
Dahlin, T., Zhou, B., 2004. A numerical comparison of 2D resistivity imaging with 10 electrode arrays. Geophys. Prospect. 52, 379–398.
Deidda, G.P., Balia, R., 2001. An ultrashallow SH-wave seismic reflection experiment on a subsurface ground model. Geophysics 66, 1097–1104.
Garambois, S., Senechal, P., Perroud, H., 2002. On the use of combined geophysical methods to assess water content and water conductivity of near-surface formation. J. Hydrol. 259, 32–48.
Harris, J.B., 1996. Shear-wave splitting in Quaternary sediments: neotectonic implications in the central New Madrid Seismic Zone. Geophysics 61, 1871–1882.
Martin, M.A., Davis, T.L., 1987. Shear-wave birefringence: a new tool for evaluating fractured reservoirs. The Leading Edge 6, 22–28.
Nelson, W.J., Denny, F.B., Follmer, L.R., Masters, J.M., 1999. Quaternary grabens in southernmost Illinois: deformation near an active intraplate seismic zone. Tectonophysics 305, 381–397.
Sanford, A.R., 1959. Analytical and experimental study of simple geologic structures. Geol. Soc. of Am. Bull. 70, 19–52.
Sexton, J.L., 2006. Lithologic and Stratigraphic Compilation of Near-Surface Sediments for the Paducah Gaseous Diffusion Plant, McCracken County, KY. Masters thesis. University of Kentucky.
Stucchi, E., Tognarelli, A., Ribolini, A., 2017. SH-wave seismic reflection at a landslide (Patigno, NW Italy) integrated with P-wave. J. Appl. Geophys. 146, 188–197.
Woolery, E.W., Almayahi, A., 2014. Shear-wave birefringence measurements in faulted near-surface sediment. Bull. Seism. Soc. Am. 104, 1540–1549.
Woolery, E.W., Street, R., 2002. Quaternary fault reactivation in the Fluorspar Area Fault Complex of western Kentucky: Evidence from shallow SH-wave reflection profiles. Seism. Res. Lett. 73, 628–639.
Woolery, E.W., Street, R.L., Wang, Z., Harris, J.B., 1993. Near-surface deformation in the New Madrid Seismic Zone as imaged by high resolution SH-wave seismic methods. Geophys. Res. Lett. 20, 1615–1618.
Woolery, E., Baldwin, J., Kelson, K., Hampson, S., Givler, R., Sundermann, S., 2009. Site-specific fault hazard assessment—Fluorspar Area Fault Complex, western Kentucky. Seism. Res. Lett. 80, 1035–1044.